Hindawi
Geofluids
Volume 2021, Article ID 4303021, 14 pages
https://doi.org/10.1155/2021/4303021

Research Article

A Control Approach of the Roof in No-Pillar Roadway Formed by Roof Cutting and Pressure Releasing

Qingnan Lou,[1] **Tingchun Li**,[1] **Qingwen Zhu**,[1] **Shanyuan Wu**,[2] **Ming Yun**,[3] **and Renle Zhao**[3]

[1]*Shandong Key Laboratory of Civil Engineering Disaster Prevention and Mitigation, Shandong University of Science and Technology, Qingdao 266590, China*
[2]*Shandong Energy Zaozhuang Mining Group Co., Ltd., Zaozhuang 277000, China*
[3]*Qiuji Coal Mine, Shandong Energy Linyi Mining Group Co., Dezhou 251105, China*

Correspondence should be addressed to Tingchun Li; tchli_sd@163.com

Received 16 April 2021; Revised 24 May 2021; Accepted 9 June 2021; Published 25 June 2021

Academic Editor: Jianwei Cheng

Roof control is one of the eternal themes of mine pressure theory, and it is also a key step of roadway formed by roof cutting. Based on the analysis of abutment pressure distribution, the viewpoint of controlling roadway roof by roof cutting distance is put forward according to the failure limit of roadway roof, and the calculation method of roof cutting distance is given. Based on the Qiuji coal mine's background, the numerical and field test study is conducted to verify the theoretical analysis, and the allowable variation range of roof cutting distance is obtained. The research shows that the roof cutting distance, abutment pressure, and roadway deformation are closely related. By controlling the roof cutting distance, the roadway roof can be placed in the low-stress area, the roadway deformation can be reduced, and the support cost can be saved. This study provides a theoretical basis for explaining the roadway's abnormal mine pressure and controlling the roadway roof by roof cutting.

1. Introduction

Coal is one of the most important energy sources, accounting for about 30% of global consumption [1]. However, due to the exploitation in past decades, coal resources are quickly exhausted, and the development of coal mining tends to improve resource recovery [2]. In the process of coal resources recovery, the protective coal pillars reserved to isolate gob for safe production have been a major cause for a low recovery rate [3]. Therefore, the gob-side entry retention technology without coal pillar is put forward and widely used. The roadway retaining along gob filling is mainly to fill artificial materials or gangue instead of coal pillars along the edge of the roadway in the mining area [4]. However, this method does not change the transfer structure of roof stress, so it is difficult to solve the problems of filling rock pillar and roadway stability, which seriously restricts its development and application [5]. Accordingly, the technology of gob-side entry retaining formed by roof cutting and pressure release [6, 7], which means drilling hole and installing explosives in the roadway roof near gob and then implementing roof presplitting with directional energizing blasting technology. After the working face passing through, the slap preventing gangue should be timely adopted to avoid the slip of broken roof into the roadway. At the same time, the gangue will fill the gob and provide support for the roof of the roadway. The principle is shown in Figure 1.

Roof cutting can change the roof structure and inevitably influence the gate road stability in the postmining stage. In the past, the roof splitting technique is mainly used to address mining accidents through blasting or hydraulic fracturing [8–11]. For example, Wang et al. [8] used deep-hole split blasting to prevent roof-weighting accidents in shallow depth seams. Wang et al. [9] applied hydraulic fracturing to address hard roof problems. Konicek et al. [10] adopted a destress-blasting method to reduce the risk of rock bursts. All of these studies suggest that transforming the rock structure is a feasible approach for controlling roof stability.

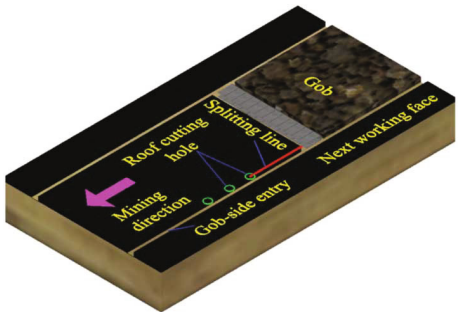

Figure 1: Schematic diagram of roadway formed by roof cutting and pressure releasing.

Besides, roof cutting is aimed at blocking the stress transfer between the working face and the roadway roof to make, the roadway be in the low-stress area. Therefore, it is a necessary condition to figure out the stress distribution of working face roof. Relevant studies have been carried out by many scholars. Zhang et al. [12, 13] mainly apply continuum theory, elastic theory, and damage mechanics to study the distribution characteristics of abutment pressure and gradually consider the effect of rock beam movement on the evolution characteristics of abutment pressure. Yu et al. [14–16] used experimental method, similar material simulation, numerical simulation, and other methods to study the distribution characteristics, influence range, peak position, and the change rule of abetment pressure with the roof's movement. Meanwhile, the microseismic monitoring and stress dynamic monitoring systems were used to reveal advanced abutment pressure distribution [17, 18]. The above research enables scholars to have a deeper understanding of the stress distribution of working face roof. However, few studies were carried out on the method of controlling the roof cutting distance, which can minimize the influence of working face roof stress on roadway roof and save the support cost. In practical engineering, the roof cutting distance is usually determined by referring to experience. However, due to the complexity and uniqueness of geological conditions, the empirical determination method is not portable.

In the present study, a calculation method of reasonable roof cutting distance to maintain the retained entry was proposed, and the roof failure mechanism and influence of roof cutting distance on the stability of roadway roof was focused on. First, the roof's stress distribution and failure mechanism were analyzed, and the calculation method of the roof cutting distance was obtained. Then, a numerical test on the influence of different roof cutting distances on the surrounding rock was carried out to verify the proposed calculation method. Meanwhile, the permissible variation range of the roof cutting distance was obtained. Finally, field tests were carried out in the Qiuji coal mine to verify the results further. The research results have positive significance to further popularizing the gob-side entry retaining technology formed by roof cutting and pressure release.

2. Roof Pressure Analysis

The advanced area of gob-side entry is affected by the mining of the working face, especially for the hard roof, the abutment pressure is large, and the influence range is wider [19]. Meanwhile, if the roof caving of the adjacent working face is not sufficient, the stress concentration will occur in the roadway's surrounding rock. Therefore, the high stress in the advanced area of the roadway makes the strong mine pressure phenomenon frequent.

Gu et al. proposed that the load of the overlying rock layer can be divided into incremental stress and uniform stress, as the solid red line shown in Figure 2 [20]. Setting this peak pressure as the boundary, its front foundation is in the elastic area, and the behind foundation is in the plastic area.

In fact, the coal body still has the bearing capacity after yielding [21], but using the exponential function to describe the advanced abutment pressure is relatively complicated. To simplify the calculation and emphasize the influence of the stress concentration factor, a multisection straight line is used to describe the advanced abutment pressure of the main roof, as the blue dotted line shown in Figure 2. Therefore, by taking the position of the coal wall as the origin of the coordinate, the load behind the peak of the abutment pressure can be obtained:

$$\sigma_z = \frac{\sigma_b - N_0}{x_b} x + N_0, \tag{1}$$

where σ_b is the maximum residual stress of the coal, MPa; N_0 is the overburden load, MPa; x_b is the length of the coal crushing zone, m.

According to experimental observations in fully mechanized caving mining, it can be known that the vertical deformation of the roof does not develop linearly but has the characteristic of the power function [22]. The yield in the elastic zone satisfies the Mohr-Coulomb criterion; therefore, the vertical elastic deformation of the main roof can be expressed by Equation (2):

$$\left.\begin{aligned} Z_1 &= a_1 x^{b_1} \\ Z_2 &= a_2 x^{b_1} \end{aligned}\right\}, \tag{2}$$

where x is the distance of a certain point, m; Z_1 is the vertical displacement, m; Z_2 is the lateral displacement, m; a_1, b_1, and a_2 are undetermined constants.

The deformation of the rock mass is related to the length in the direction of applied force. However, there are rock layers above and below the main roof to limit its vertical deformation. Therefore, only the influence of the load on the main roof's deformation is considered. According to the Mohr-Coulomb criterion in the elastic state [23], we can get

$$a_2 = \frac{a_1}{\alpha}, \tag{3}$$

where $\alpha = \nu/1 - \nu tg^2(45^\circ + \varphi/2) + 1$.

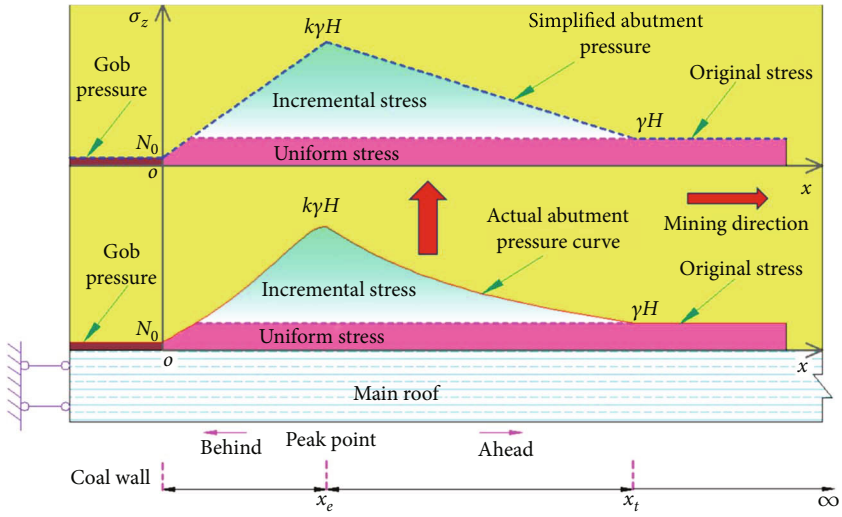

Figure 2: Schematic diagram of roof abutment pressure.

According to the ratio of transverse strain to the vertical strain of the roof, the length of the elastic area can be obtained:

$$\Delta x = \frac{h(1-\nu)}{\nu^2 tg^2(45^\circ + (\varphi/2)) + \nu - \nu^2}, \tag{4}$$

where ν is the rock's Poisson's ratio.

By substituting the peak point pressure ($K\gamma H$) into Equation (1), the distance between the peak point and the working face can be obtained. Then combining with Equation (4), when the abutment pressure is restored to the original rock stress, the distance between the working face and the position can be obtained. Equation (5) can be obtained according to the pressure and position of the peak point and the position where the abutment pressure reaches the original rock stress.

$$\sigma_z = k\gamma H + \frac{(k-1)\gamma H\left[\nu^2 tg^2(45^\circ + (\varphi/2)) + \nu - \nu^2\right]}{h(\nu - 1)} \cdot \left[x - \frac{x_b(k\gamma H - N_0)}{\sigma_b - N_0}\right] \tag{5}$$

Equations (1) and (5) can describe the roof bearing pressure distribution, which lays a foundation for roof pressure analysis.

3. Roof Model Establishment and Motion Law Analysis

3.1. Stress Model of Roadway's Main Roof. The roof above the working face and the roof above the roadway are integral structures before the roof cutting [24], so the roof's pressure distribution is the same. However, the existence of a roadway causes the stress to be released or transferred through the deformation of the surrounding rock [25]. Meanwhile, after roadway excavation, the immediate roof usually deforms greatly and is separated from the main roof. Under the influence of mining, the separation will be further intensified so that the immediate roof cannot support the main roof [26]. Besides, related studies show that the bearing capacity of the hard roof is strong, and the advanced area can be supported only by a hydraulic prop or without support [27]. However, the hydraulic prop cannot act directly on the main roof, so it cannot restrict the main roof's deformation and fracture [28].

Based on the above analysis, it is assumed that (1) the main roof of the roadway does not deform. (2) The roof cutting distance is smaller than the influence range of advanced abutment pressure. As shown in Figure 3, the force model of the main roof is established where q_0 is the stress of the main roof; q_s is the stress of primary rock; t is the abutment pressure coefficient; h is the main roof's thickness.

Because the roadway roof and the working face roof are cut off by roof cutting, the roof stress transmission can be cut off effectively; thus, the roof cutting area will not be affected by the advanced abutment pressure. The small stress of the roadway roof and the stable surrounding rock helps achieve excellent gob-side entry retaining automatically formed by roof cutting and pressure release. The section's roadway roof is not the focus of this article, so its mechanical characteristics will not be described in detail.

For the uncut roof area, part of the main roadway roof is within the influence range of the advanced abutment pressure, as shown in Figure 3. Taking the unit width within the influence range of advanced abutment pressure, and taking the sum of the width of the roadway and the length of roof fracture in the solid coal as the length of the rocking beam, the beam model of the main roof with fixed-supported at both ends can be established, as shown in the dashed box in Figure 3.

3.2. Analysis of the Failure Process of the Main Roof of the Roadway. The mechanical model of dotted frame in

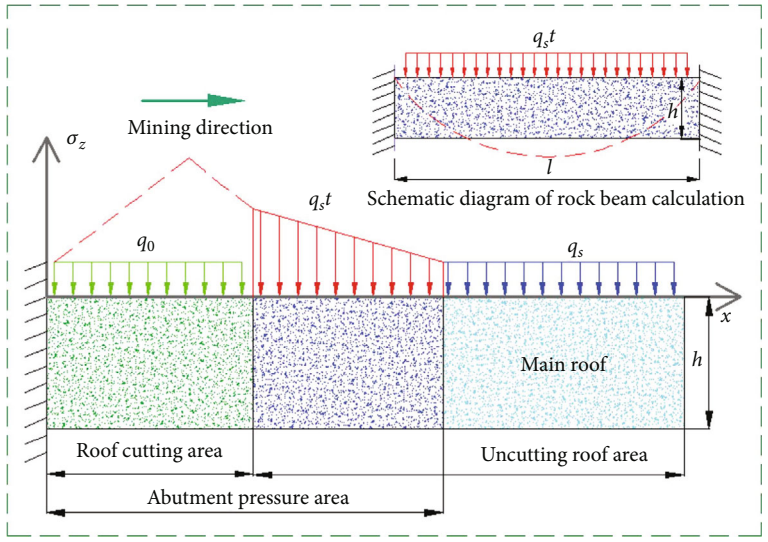

Figure 3: Strike direction main roof force model.

Figure 3 is taken as the research object, and the deflection formula under vertical load (including own weight) is

$$\omega = -\left(q_s t + \gamma_j h\right)\frac{y^2(y-l)^2}{24EI}, \tag{6}$$

where E is the elastic modulus of the main roof, GPa; I is the inertia moment of the rock beam section, m^4; γ_j is bulk density of the main roof, kN/m^3; y is the distance to one side of the beam, m; l is the length of the fixed beam, m.

Under the action of external force, both ends of the fixed beam will appear stress concentration, which will lead large shear stress and tensile stress to reach the allowable stress easily [29, 30]. Then, the tensile failure will occur at both ends of the fixed beam, and the tensile stress at the end is

$$\sigma = \frac{M}{W}, \tag{7}$$

where M is the bending moment of the middle part of the roadway roof, N·m; W is the bending section coefficient of the roadway roof, $W = h^2/6$.

The vertical force is regarded as the uniform load, and the bending moment at the end of the fixed beam at both ends can be obtained by structural mechanics as follows:

$$M = \frac{1}{12}\left(q_s t + \gamma_j h\right)l^2. \tag{8}$$

By substituting Equation (8) into Equation (7), the tensile stress when the ends of the fixed beams fail is

$$\sigma = \frac{\left(q_s t + \gamma_j h\right)l^2}{2h^2}. \tag{9}$$

When the tensile stress at the end is greater than the allowable stress, the fixed end will undergo tensile failure,

Table 1: Criteria for judging roadway roof state.

State of rock beam	Fixed two end beam	Critical state	Simply supported beam	Critical state	Failure
t	$t < t_g$	$t = t_g$	$t_g < t < t_z$	$t = t_z$	$t > t_z$
ω	$\omega < \omega_g$	$\omega = \omega_g$	$\omega_g < \omega < \omega_z$	$\omega = \omega_z$	$\omega > \omega_z$

and the fixed rock beam will be transformed into a simple support beam. At this time, let $t = t_g$, then t_g is

$$t_g = \frac{2h^2[\sigma_t] - \gamma_j h l^2}{q_s l^2}. \tag{10}$$

The end of the simply supported beam cannot bear tensile stress, and the maximum tensile stress is transferred to the middle and lower edge of the rock beam. At the same time, the pressure will be released after the failure of the fixed end. Here, the vertical load is 1/2 of the original load. The deflection formula and the tensile stress at the bottom edge of the middle part of the simple support rock beam can be obtained as follows:

$$\begin{aligned}\omega &= -\left(q_s t + \gamma_j h\right)\frac{\left(y^4 - 2ly^3 + l^3 y\right)}{48EI},\\ \sigma &= \frac{3\left(q_s t + \gamma_j h\right)l^2}{8h^2}.\end{aligned} \tag{11}$$

When tensile failure occurs at the middle and lower edge of a simply supported beam, let $t = t_g$, then t_z is

$$t_z = \frac{8[\sigma_t]h^2 - 3l^2\gamma_j h}{3q_s l^2}. \tag{12}$$

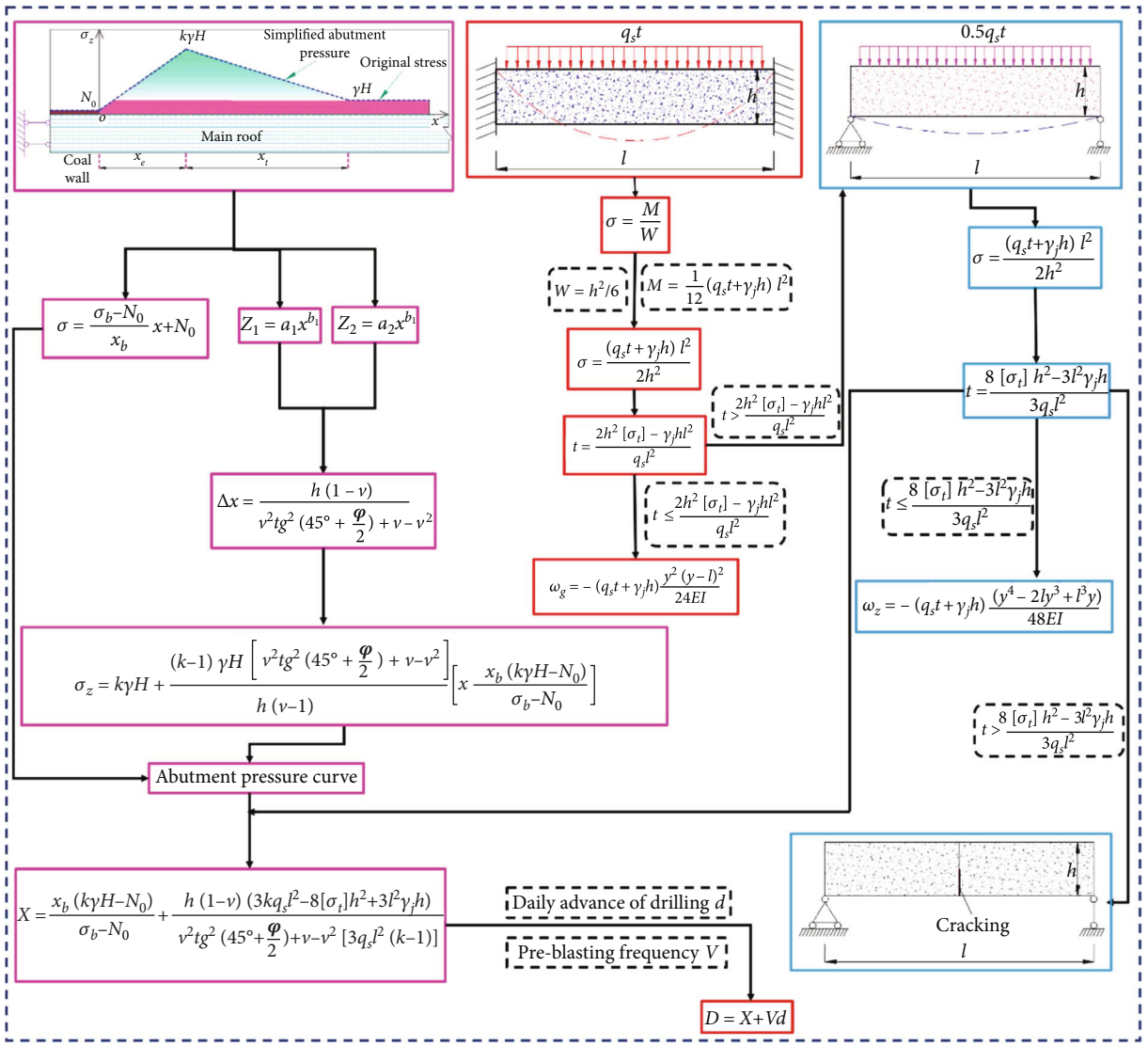

Figure 4: Flow chart of the derivation of the roof cutting distance.

When $t = t_g$, $\omega = \omega_g$; when $t = t_z$, $\omega = \omega_z$; the judgment criteria of roadway main roof structure can be obtained, as shown in Table 1.

3.3. Determination of the Roof Cutting Distance. According to Equation (12), the roof failure abutment pressure coefficient can be obtained. Combined with Equation (5), the distance (X) from the farthest failure site to the working face can be obtained as:

$$X = \frac{x_b(k\gamma H - N_0)}{\sigma_b - N_0} + \frac{h(1-\nu)}{\nu^2 tg^2(45° + (\varphi/2)) + \nu - \nu^2} \times \frac{3kq_s l^2 - 8[\sigma_t]h^2 + 3l^2\gamma_j h}{3q_s l^2(k-1)} \quad (13)$$

However, the advanced abutment pressure moves forward with the coal seam mining, and the daily mining length and roof cutting frequency should also be considered. Determine the roof cutting distance (D) as follows:

$$D = X + Vd, \quad (14)$$

where V is the advanced cutting frequency; d is the daily mining progress, m.

In order to summarize the derivation of the pressure distribution of the advanced abutment pressure and the advanced cutting distance and relationship between formulas, the derivation flowchart is given in Figure 4.

4. Simulation Test of Roof Motion Law

Based on the above analysis, this paper will use numerical simulation to analyze the advanced abutment pressure distribution of the main roof. Meanwhile, the vertical displacement of the roadway roof and the change law of the plastic

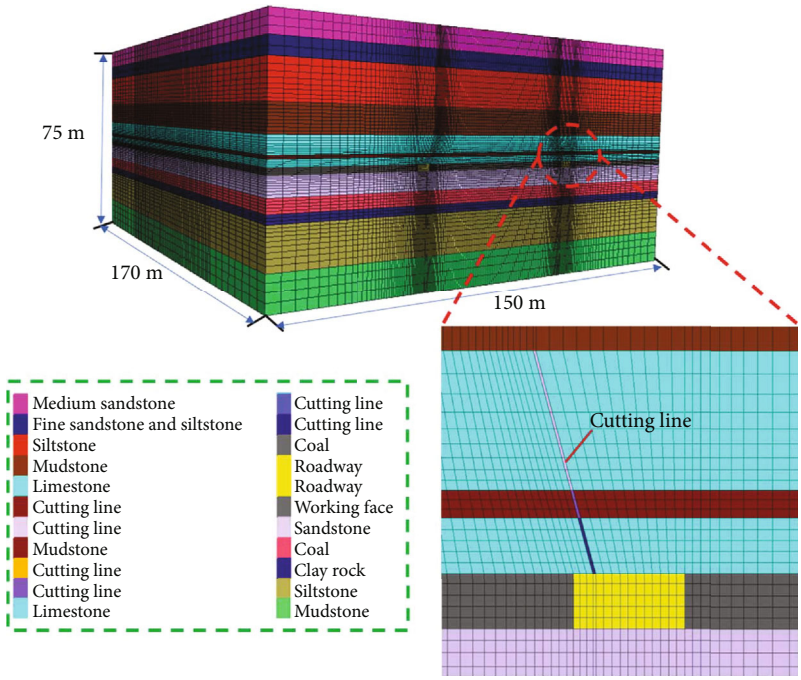

Figure 5: Numerical model.

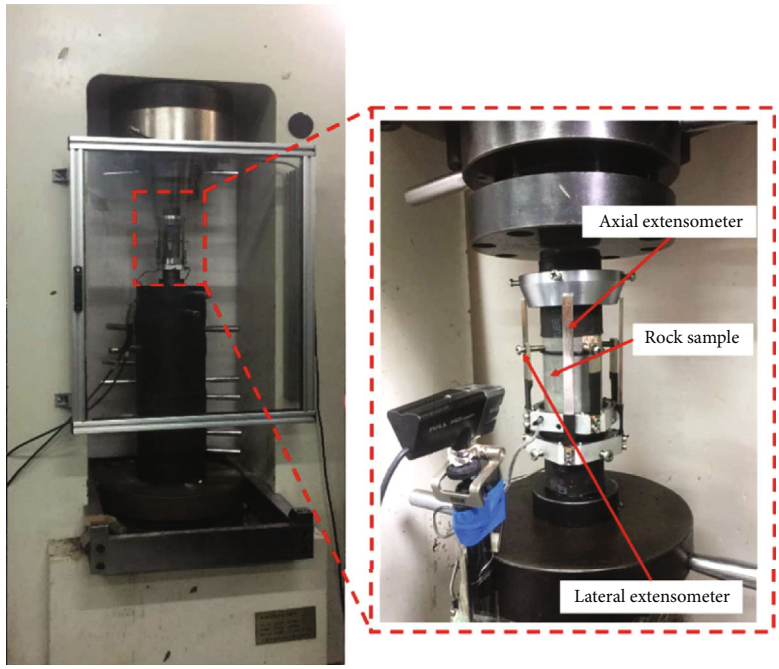

Figure 6: Rock mechanic parameter test.

zone under different roof cutting distances will also be analyzed. Then, the optimal roof cutting distance can be determined.

4.1. Model. FLAC^{3D} simulation software is used to establish a numerical calculation model, as shown in Figure 5. The model size is 170 m (length) × 150 m (width) × 75 m (height), the roadway height is 2 m, width is 4 m, and the vertical height of the cut seam is 8 m with an angle of 15°. The vertical downward stress is applied to the upper boundary of the model, the bottom is fixed, and both sides' horizontal displacement is restricted [31, 32]. The Mohr-Coulomb model is adopted. The material parameters of the rocks are selected based on geological conditions in Section 5.1. Rock samples are collected from the site, as shown in Figure 6, and the rock parameter mechanics experiment is conducted, so as to obtain rock mechanical parameters, as shown in Table 2.

Table 2: Physical and mechanical parameters of coal.

Lithology	Bulk modulus (GPa)	Shear modulus (GPa)	Tensile strength (MPa)	Cohesion (MPa)	Internal friction angle (°)	Density ($kg \cdot m^{-3}$)
Medium sandstone	7.21	4.8	1.2	2.8	27	2560
Siltstone	4.3	2.1	1.8	1.5	27	2630
Mudstone	2.8	1.1	1.1	1.5	23	2250
Limestone	5.4	2.8	4.5	3.1	28	2650
Coal	0.9	0.6	0.8	1	23	1420

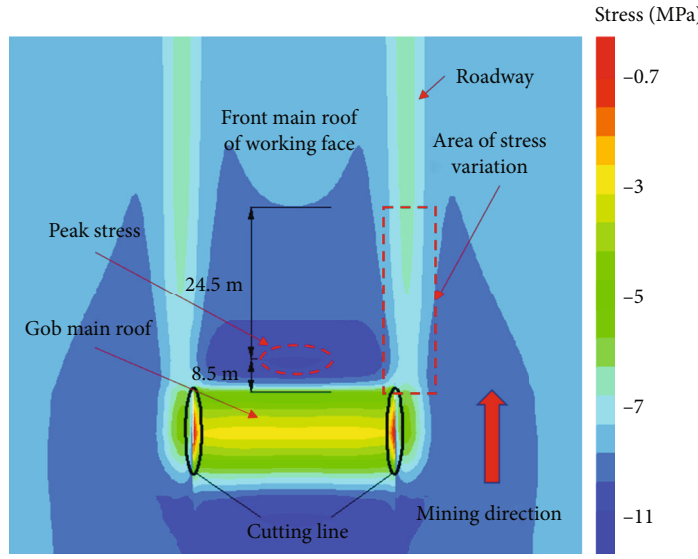

Figure 7: The distribution of advanced abutment pressure.

4.2. Distribution Law of Abutment Pressure. Figure 7 illustrates a cloud diagram of the advanced abutment pressure after 20 m of working face excavation.

It can be seen from Figure 7 that the advanced abutment pressure of the main roof of the working face increased rapidly to a peak of about 12.1 MPa at about 8.5 m in front of the coal wall. Then, the advanced abutment pressure dropped to 7.2 MPa about 33 m from the working face, equaling to the stress of primary rock. At the same time, the main roof above the roadway started to grow from the position of the coal wall, reached a peak at 8.5 m in front of the coal wall, and then began to fall until reaching a smooth at about 33 m in front of the coal wall. The results show that the change law is the same as the theoretical analysis.

4.3. Influence of Roof Cutting Distance on Roof Movement

4.3.1. Determination of the Lower Limit of Roof Cutting Distance

(1) Simulation Results of Vertical Displacement of Roadway Roof. The vertical displacement of the roof of the roadway in the uncut roof area under the condition of different roof cutting distances was simulated, and the measuring points were arranged at 2 m, 5 m, 10 m, 15 m, and 20 m in front of the roof cutting area. The simulation results are shown in Figure 8.

(1) When the roof was cut 10 m ahead, the vertical displacement of the main roof at 2 m, 5 m, and 10 m in front of the roof cutting area was 42 mm, 37 mm, and 30 mm; and the vertical displacement of the immediate roof was 45 mm, 38 mm, and 35 mm, respectively; the vertical displacements were both relatively large. The vertical displacements of the main roof at 15 m and 20 m in front of the roof cutting area was 12 mm and 9 mm, respectively, and the vertical displacements of the immediate roof were 17 mm and 15 mm, respectively, the vertical displacements were both small.

(2) When the roof was cut 16 m ahead, at 2 m in front of the roof cutting area, the vertical displacement of the main roof and the immediate roof was 26 mm and 32 mm, respectively, which is a large vertical displacement. From 5 m to 20 m ahead of the

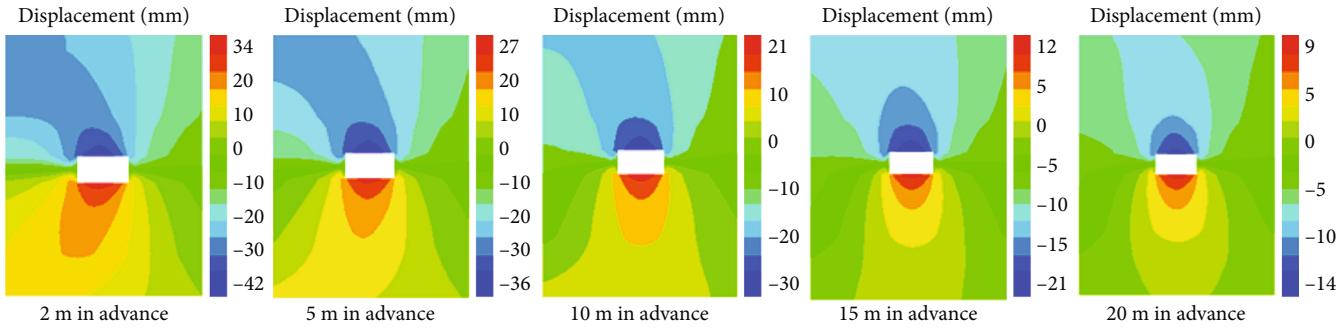

(a) Roof cutting 10 m

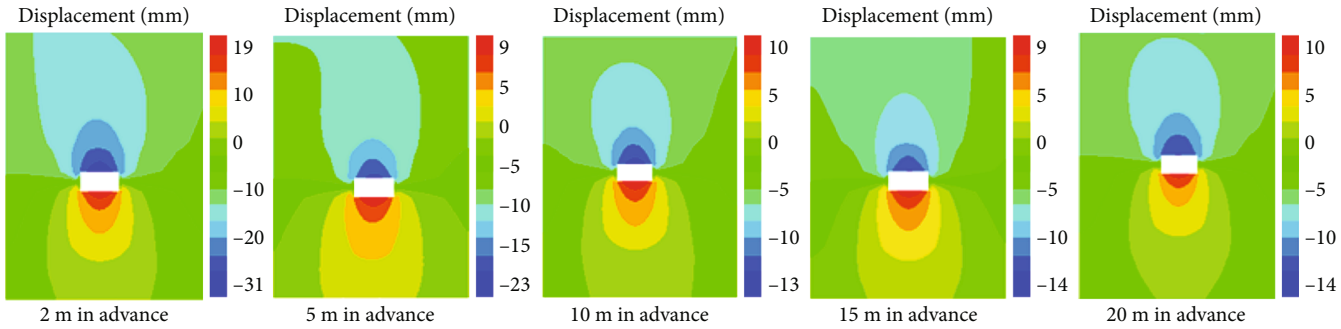

(b) Roof cutting 16 m

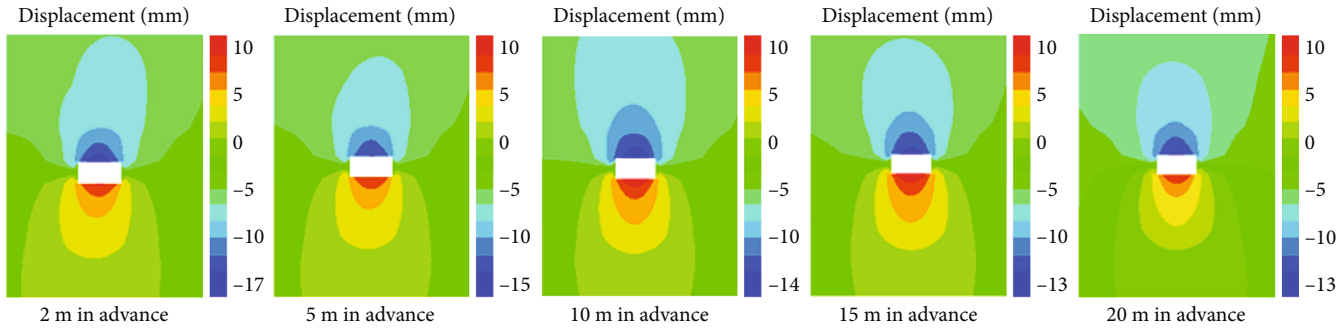

(c) Roof cutting 21 m

Figure 8: Simulation test results of roof displacement.

roof cutting area, displacement of the main roof was reduced from 13 mm to 8 mm, while the vertical displacement of the immediate roof was reduced from 19 mm to 12 mm; the vertical displacement of the roof was small.

(3) When the roof was cut 21 m ahead, the vertical displacement of the roadway roof in front of the roof cutting area was small, the vertical displacement of the immediate roof was about 14 mm, and the vertical displacement of the main roof was about 8 mm.

From the above analysis, it can be seen that when the roof was cut 21 m ahead, the impact of the high-stress area of the advanced abutment pressure on the roadway roof can be avoided.

(2) Simulation Results of the Plastic Area of Surrounding Rock of Roadway Roof. Under different roof cutting distances, the plastic zone change in the uncut roof area was simulated. The plastic zone of the roadway at 2 m, 5 m, 10 m, 15 m, and 20 m in front of the roof cutting area was analyzed. The simulation results are shown in Figure 9.

According to Figure 9, when the roof cutting is 10 m in advance, in the range of 15 m in front of the roof cutting area, the area of solid coal of the roadway reentering the plastic zone is larger, and the area of reentering the plastic zone is smaller after 15 m. When the roof cutting is 16 m in advance, in the range of 5 m in front of the roof cutting area, the area of solid coal of the roadway reentering the plastic zone is larger, and the area of reentering the plastic zone is smaller after 5 m. When the roof cutting is 21 m in advance, the area of solid coal reentering the plastic zone in the roadway ahead of the roof cutting area is small.

According to the above analysis, it can be concluded that when the roof is cut 21 m in advance, the roof stress in front of the roof cutting area is small, which is conducive to the

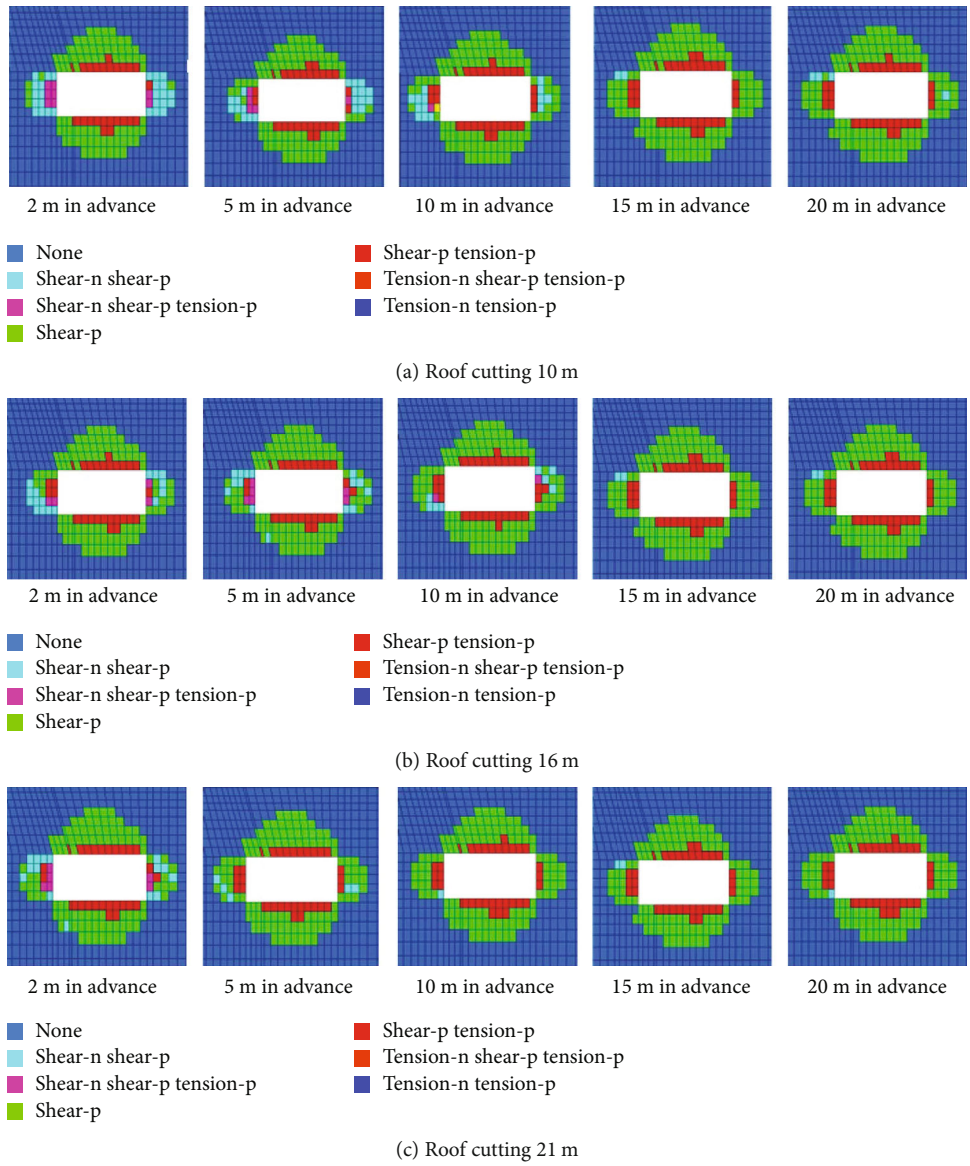

Figure 9: Simulation test results of plastic area.

stability of the roadway roof and surrounding rock, realizing excellent gob-side entry.

4.3.2. Determination of the Upper Limit of the Roof Cutting Distance. The roof cutting reduces the vertical constraint on the roadway roof and makes the roadway roof become a cantilever structure [33], which is easy to produce a large vertical displacement at the cantilever end and affect the effect of the gob-side entry. To highlight the roof deformation law in the cut area of the roadway roof, the vertical displacement of the roof of the roadway without support in the mining area was simulated under the condition of different cutting distances of the roadway roof. The cantilever displacement with the largest variation is taken as the reference quantity, and its variation rule is shown in Figure 10.

It can be seen from Figure 10 that with the increase of the advanced cutting distance, the vertical displacement of the roadway roof in the cutting area gradually increased. However, when the roof cutting distance was within 0-30 meters, the deformation of the roof increased slowly. When the roof cutting distance was more than 30 m, the deformation of the roof increased faster. Especially for the immediate roof, the deformation increase was more obvious.

By comprehensively comparing and analyzing, it is indicated that roof cutting can reduce advanced abutment pressure on the roadway roof. However, the vertical displacement of the roadway roof in the roof cutting area increases with the roof cutting distance. When the cutting distance was 21 m, the influence of the advanced abutment pressure can be effectively avoided, and the roof deformation was small. In the 1102 working face of the Qiuji coal mine, 6.4 m is mined and cut roof every day, so the roof cutting distance is determined to be 27.4 m. Meanwhile, the distance of roof cutting can be adjusted according to the site construction, but it

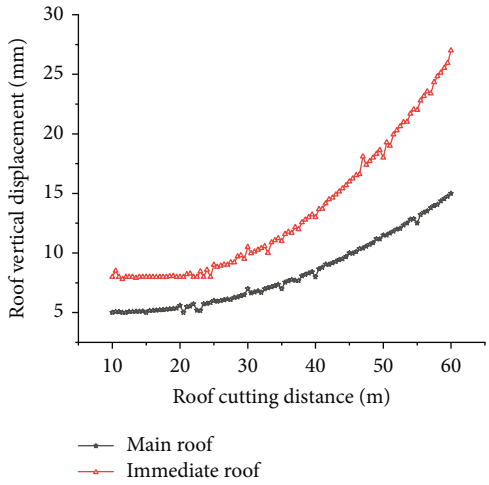

Figure 10: Relationship between roof cutting distance and roof displacement in roof cutting area.

cannot be reduced, and the increased length is best controlled within 2.6 meters.

5. Engineering Verification

5.1. Geological Conditions. The lower group of coal in the Yellow River North Coalfield cannot be mined because of the Ordovician water, and nearly 10 billion tons of coal resources need to be liberated. Qiuji coal mine belongs to the Yellow River North Coalfield and is located in Jining City, Shandong Province, China, and it has nearly 200 million tons of coal to be liberated. Therefore, the roof and floor of 11 coal were grouted in the Qiuji coal mine, to be mined. The working face 1102 is the first mining test face, and its mining mode is of great significance to the subsequent coal mining. The buried depth of 1102 working face is $H = 420 \sim 470$ m, the width is 52 m, and the length is 173 m. The coal seam's thickness is 1.86~2.45 m with an average of 2.02 m, and the coal seam inclination is 3°~8° with an average of 4°. The immediate roof consists of mudstone (upper part) and limestone (lower part) with an average thickness of 1.14 m for mudstone and 2.01 m for limestone. The main roof is limestone with an average thickness of 5.13 m. The immediate roof and the main roof belong to the hard roof with excellent integrity, which causes the roadway's surrounding rock to be greatly affected by the dynamic pressure of the working face. The immediate bottom is siltstone with a thickness of 5.56 m, and the 13 coal is under the immediate bottom with an average thickness of 5.56 m. The plan of 1102 working face and columnar view of roof and floor strata are shown in Figure 11.

5.2. Theoretical Calculation Results. Taking 1102 working face of Qiuji coal mine as the background, the relevant parameters are as follows: $x_b = 1.5$ m, $\sigma_b = 4.12$ MPa, $N_0 = 2.4$ MPa, $\nu = 0.15$, $\gamma = 17.9$ kN/m^3, $\gamma_j = 26.5$ kN/m^3, $H = 380$ m, $\varphi = 28°$, $h = 5.13$ m, $q_s = 6.8$ MPa, $E = 95$ GPa, $V = 1$, $d = 6.4$, and the parameters of sinking curve of the main roof is $a_1 = 0.008$, $b_1 = 2$. According to the study of the stress of the upper roof of the coal seam, the main roof's stress concentration is less than the coal seam, and the peak abutment pressure decreases with the vertical distance [34]. Therefore, k is set as 1.9. Meanwhile, considering that fissures in the rock reduce the rock's strength, and the fracture of the main roof occurs at the roadway side inside the coal [35, 36]. So, take $[\sigma_t] = 3.5$ MPa, $l = 5$ m.

By substituting the parameters into Equations (1), (5), (13), and (14), the following equation can be obtained: the peak advanced abutment pressure of the main roof is 12.92 MPa, which appears 9.16 m ahead of the working face, and its influence range is 32.43 m ahead of the coal wall. The advanced cutting distance is 27.45 m. The theoretical calculation results are in good agreement with the simulation results.

5.3. Monitoring Point Layout. According to the above result, the roof cutting distance is determined to be 28 m, and the field test is carried out in the 1102 working face of the Qiuji coal mine. In order to verify the research results, monitoring points are arranged in the roadway to monitor the roadway surface displacement and roof separation and anchor axial force in the process of mining, and the overall effect of roof cutting is analyzed. The layout of monitoring points is shown in Figure 12.

In Figure 12, subfigure a is the roof separation sensor and anchor cable dynamometer to monitor the roof separation amount and anchor cable axial force. The deep base point and the shallow base point represent the installation positions of the two fluke of the roof separation sensor, and the separation amount of the roof below the fluke is monitored, respectively. Subfigure b is the roof and floor dynamic sensor to monitor the convergence of the roof and floor. Subfigure c is the laser range finder, monitoring the convergence of the roadway side.

5.4. Roadway Surface Displacement. The surface monitoring displacement curve is shown in Figure 13. It shows that the advanced abatement pressure has little influence on the roadway, and the roof and roadway side begin to deform at 15 m in the advanced working face. However, the roadway roof subsidence and roadway side displacement are both small, while the values are 12 mm and 8 mm, respectively. In the range of 0 ~ 18 m behind the working face, the roadway deformation is severe, and the deformation increases rapidly. When the working face is 18~ 40 m behind, with the gob roof compaction, the roadway deformation rate decreases until it tends to be stable. Finally, the roadway's roof subsidence is about 55 mm, and the roadway side displacement is about 41 mm. In conclusion, the roadway's deformation is small, the surrounding rock is stable, and the effect of retaining the roadway is excellent.

5.5. Roof Separation. Figure 14 shows the change curve of the roof separation of the on-site monitoring roadway. The vertical red dotted line in the figure is the installation position of the roof separation sensor in the roadway.

It can be seen from Figure 14 that with the working face gradually close to the monitoring point, the separation

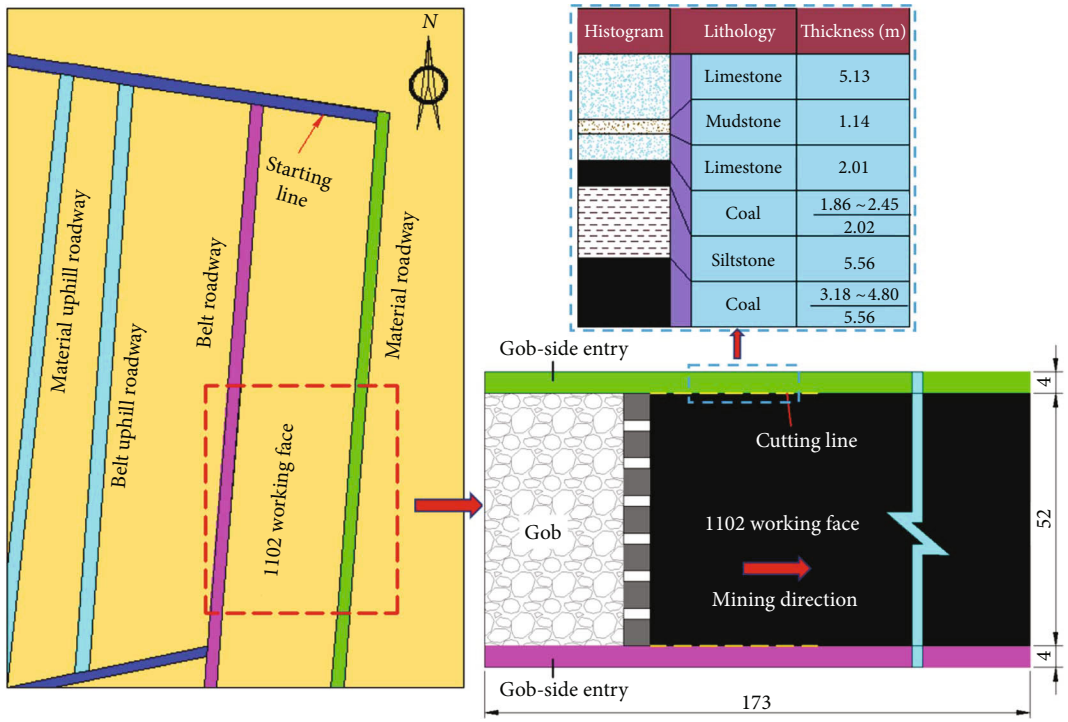

Figure 11: Plan view of 1102 working face and columnar view of roof and floor strata.

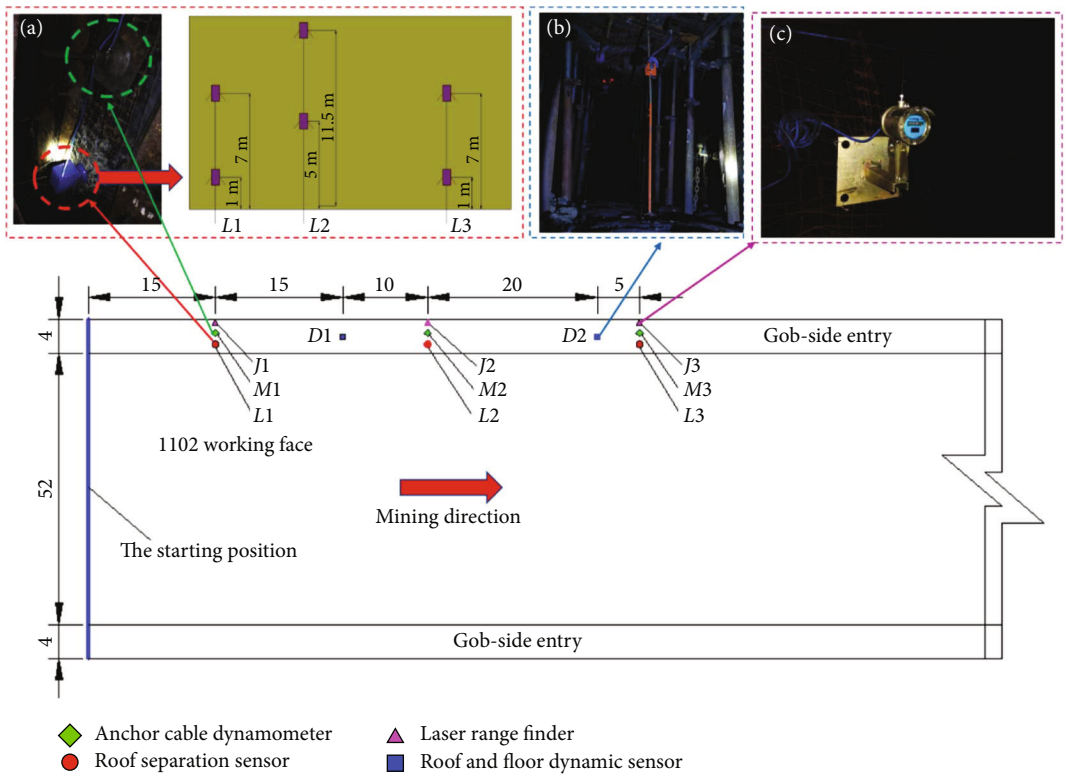

Figure 12: Roadway monitoring point layout.

amount of roadway roof in the cutting roof area and the uncutting roof area were both small. After the working face passed the monitoring point for a certain distance, the separation amount of the roadway roof suddenly increased, induced by the collapse of the immediate roof and the main roof of the working face. By setting the immediate roof

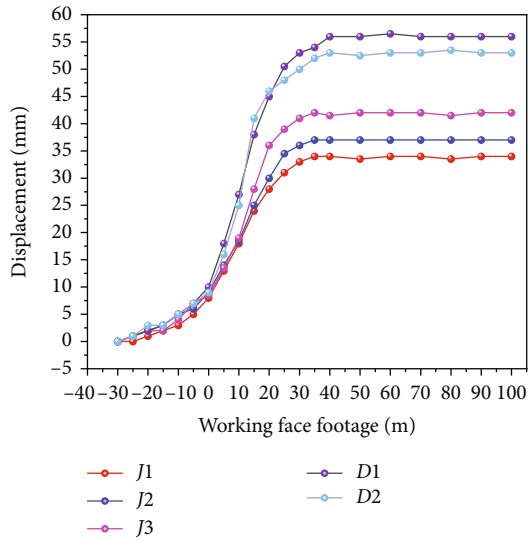

Figure 13: Displacement curve of the roadway surface.

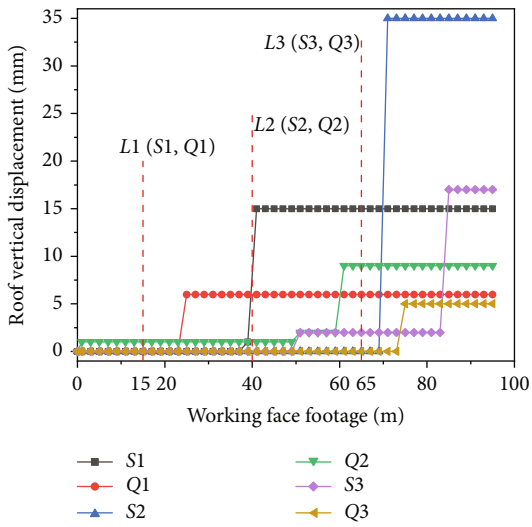

Figure 14: Separation curve of roadway roof.

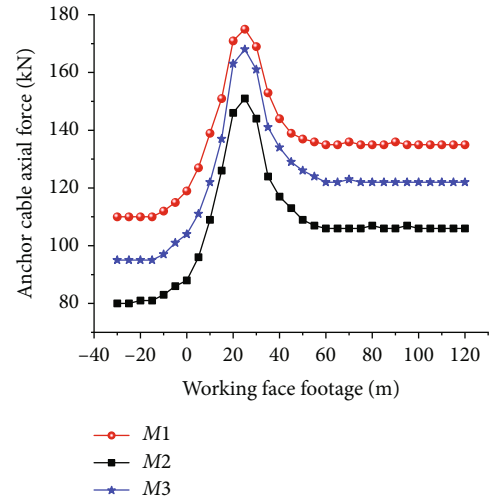

Figure 15: Variation law of roof anchor cable axial force.

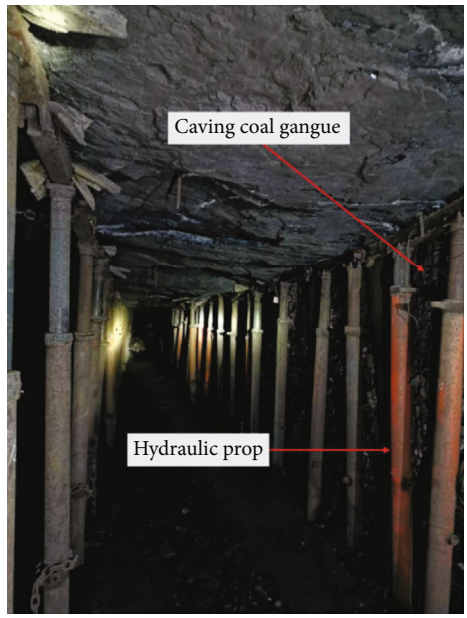

Figure 16: Renderings of gob-side entry.

surface as the origin, the total convergence of the roadway roof from 0 to 1 m is 6 mm, 9 mm for the roadway roof from 0 to 5 m, 15 mm for the roadway roof from 0 to 7 m, and 35 mm the roadway roof from 0 to11.5 m. According to the above analysis, it was indicated that the smaller convergence of the roadway roof is, and the more stable the surrounding rock is, which verifies the reliability of the roof cutting distance obtained by theoretical calculation.

5.6. Monitoring of Roadway Roof Anchor Cable Axial Force. The axial force variation of roadway roof anchor cable is shown in Figure 15.

As can be seen from Figure 15, when about 15 m in front of the working face, the anchor cable axial force begins to increase, and when about 25 m behind the working face, it increases to the peak value. The gob roof deforms and caving behind the working face at 0 ~ 25 m resulted in the rapid increase of anchor cable pressure. After 25 m behind the working face, the anchor cable axial force gradually decreased and finally stabilized with the gradual compaction of the gob roof. When the anchor cable axial force is stable, it indicates that the gob roof has caved outside the cut suture and is compacted. Meanwhile, the peak value of the anchor cable axial force is relatively small, which indicates that the pressure relief effect of the roadway is excellent. The actual situation on-site (Figure 16) also indicated that after the working face's progress, gob-side entry retaining formed by roof cutting and pressure release was successfully realized.

6. Conclusion

In this paper, a method of controlling the stability of the roadway roof by changing the cutting distance is put forward. The main research conclusions are as follows:

(1) According to the roof pressure distribution, a mechanical model of roadway roof is established, and the evolution process of roof failure is summarized: fixed beam at both ends → simply supported beam → failure. Meanwhile, the critical criterion of structure evolution is given. Combined with the abutment pressure distribution curve, the roof's furthest failure position in front of the working face is obtained. The optimal roof cutting distance is the daily mining length multiply roof cutting frequency and then plus the length from the furthest failure point to the working face.

(2) The roof cutting distance, advanced abutment pressure, and roadway deformation are closely related. The roof cutting distance is small, and the roof of the gob-side entry is damaged under the action of advanced abutment pressure. With the roof cutting distance increase, the roof deformation of the gob-side entry in the cutting area increases. Based on the calculated results, the roof deformation in the cut roof area increases slightly when the roof cutting distance increases within the range of 2.6 m. However, the reduction of the roof cutting distance will result in large deformation of the roof in the uncut area.。

(3) Engineering verification is conducted in 1102 gob-side entry in Qiuji coal mine. The monitoring results and the field application effect show that the roadway convergence is small, and the pressure relief effect is significant. Therefore, the feasibility and effectiveness of the calculation approach are verified.

Data Availability

Data used in this article are available through email from the corresponding author.

Conflicts of Interest

The authors declare no conflicts of interest.

Authors' Contributions

Writing and original draft preparation was done by Q.L. and T.L., methodology was done by Q.Z., formal analysis: R.Z., investigation was done by M. Y and S.W., and software was done by Q.L. and Q.Z. All authors have read and agreed to the published version of the manuscript.

Acknowledgments

This study was supported by the National Natural Science Foundation of China (No. 41772299).

References

[1] Y. B. Gao, Y. J. Wang, J. Yang, X. Y. Zhang, and M. C. He, "Meso- and macroeffects of roof split blasting on the stability of gateroad surroundings in an innovative nonpillar mining method," *Tunneling & Underground Space Technology*, vol. 90, pp. 99–118, 2019.

[2] Z. G. Tao, C. Zhu, M. C. He, and M. Karakus, "A physical modeling-based study on the control mechanisms of negative Poisson's ratio anchor cable on the stratified toppling deformation of anti- inclined slopes," *International Journal of Rock Mechanics and Mining Sciences*, vol. 138, p. 104632, 2021.

[3] C. Zhu, M. C. He, M. Karakus, X. H. Zhang, and Z. G. Tao, "Numerical simulations of the failure process of anaclinal slope physical model and control mechanism of negative Poisson's ratio cable," *Bulletin of Engineering Geology and the Environment*, vol. 80, no. 4, pp. 3365–3380, 2021.

[4] Y. Wang, W. K. Feng, R. L. Hu, and C. H. Li, "Fracture evolution and energy characteristics during marble failure under triaxial fatigue cyclic and confining pressure unloading (FC-CPU) conditions," *Rock Mechanics and Rock Engineering*, vol. 54, no. 2, pp. 799–818, 2021.

[5] B. Li, R. Bao, Y. Wang, R. Liu, and C. Zhao, "Permeability evolution of two-dimensional fracture networks during shear under constant normal stiffness boundary conditions," *Rock Mechanics and Rock Engineering*, vol. 54, no. 1, pp. 409–428, 2021.

[6] M. C. He, G. L. Zhu, and Z. B. Guo, "Longwall mining "cutting cantilever beam theory" and 110 mining method in China–the third mining science innovation," *Journal of Rock Mechanics and Geotechnical Engineering*, vol. 7, no. 5, pp. 483–492, 2015.

[7] Q. Wang, M. He, J. Yang, H. Gao, B. Jiang, and H. Yu, "Study of a no-pillar mining technique with automatically formed gob-side entry retaining for longwall mining in coal mines," *International Journal of Rock Mechanics and Mining Sciences*, vol. 110, pp. 1–8, 2018.

[8] Q. Wang, H. K. Gao, B. Jiang, S. C. Li, M. C. He, and Q. Qin, "In-situ test and bolt-grouting design evaluation method of underground engineering based on digital drilling," *International Journal of Rock Mechanics and Mining Sciences*, vol. 138, p. 104575, 2021.

[9] Q. Wang, Q. Qin, B. Jiang et al., "Mechanized construction of fabricated arches for large-diameter tunnels," *Automation in Construction*, vol. 124, p. 103583, 2021.

[10] P. Konicek, K. Soucek, L. Stas, and R. Singh, "Long-hole destress blasting for rockburst control during deep underground coal mining," *International Journal of Rock Mechanics and Mining Sciences*, vol. 61, pp. 141–153, 2013.

[11] B. Huang, Y. Wang, and S. Cao, "Cavability control by hydraulic fracturing for top coal caving in hard thick coal seams," *International Journal of Rock Mechanics and Mining Sciences*, vol. 74, pp. 45–57, 2015.

[12] Q. Zhang, C. H. Peng, R. C. Liu, B. S. Jiang, and M. M. Lu, "Analytical solutions for the mechanical behaviors of a hard roof subjected to any form of front abutment pressures," *Tunneling & Underground Space Technology*, vol. 85, pp. 128–139, 2019.

[13] A. Li, Q. Ma, L. Ma, L. Kang, Q. Mu, and J. B. Chen, "Coal mine abutment pressure distribution based on a strain-softening model," *Frontiers in Physics*, vol. 8, 2020.

[14] B. Yu and L. F. Zhang, "Study on the abutment pressure distribution in top coal caving," *Arabian Journal of Geosciences*, vol. 13, no. 4, 2020.

[15] J. Q. Jiang, P. Wang, P. Q. Zheng, and Q. L. Wu, "Evolution characteristics of mining-induced fracture and abutment stress under high-position hard thick stratum and its effect on gas migration," *Journal of Mining and Safety Engineering*, vol. 34, pp. 624–631, 2017.

[16] M. Eremina, G. Esterhuizenb, and I. Smolinac, "Numerical simulation of roof cavings in several Kuzbass mines using finite- difference continuum damage mechanics approach," *International Journal of Mining Science and Technology*, vol. 30, no. 2, pp. 157–166, 2020.

[17] S. T. Zhu, Y. Feng, and F. X. Jiang, "Determination of abutment pressure in coal mines with extremely thick alluvium stratum: a typical kind of rockburst mines in China," *Rock Mechanics and Rock Engineering*, vol. 49, no. 5, pp. 1943–1952, 2016.

[18] W. Cai, X. X. Bai, G. Y. Si, W. Z. Cao, S. Y. Gong, and L. M. Dou, "A monitoring investigation into rock burst mechanism based on the coupled theory of static and dynamic stresses," *Rock Mechanics and Rock Engineering*, vol. 53, no. 12, pp. 5451–5471, 2020.

[19] Y. Y. Lu, T. Gong, B. W. Xia, B. Yu, and F. Huang, "Target stratum determination of surface hydraulic fracturing for far-field hard roof control in underground extra-thick coal extraction: a case study," *Rock Mechanics and Rock Engineering*, vol. 52, no. 8, pp. 2725–2740, 2019.

[20] S. T. Gu, B. Y. Jiang, Y. Pan, and Z. Liu, "Bending moment characteristics of hard roof before first breaking of roof beam considering coal seam hardening," *Shock & Vibration*, vol. 2018, article 7082951, 22 pages, 2018.

[21] F. Q. Gong, Y. L. Wang, Z. G. Wang, J. F. Pan, and S. Luo, "A new criterion of coal burst proneness based on the residual elastic energy index," *International Journal of Mining Science and Technology*, 2021.

[22] Z. H. Chen and H. P. Xie, "Damage mechanics analysis of abutment pressure distribution in fully mechanized coal mining stope," *Chinese Journal of Rock Mechanics and Engineering.*, vol. 19, pp. 436–439, 2000.

[23] X. P. Chen, "Study on the ultimate bearing capacity of rock foundation based on Mohr-Columb criterion Chinese," *Journal of Underground Space and Engineering*, vol. 12, pp. 95–99, 2016.

[24] H. L. Zhang, M. Tu, H. Cheng, and Y. Z. Tang, "Breaking mechanism and control technology of sandstone straight roof in thin bedrock stope," *International Journal of Mining Science and Technology*, vol. 30, no. 2, pp. 259–263, 2020.

[25] F. Q. Gao, H. P. Kang, and L. Yang, "Experimental and numerical investigations on the failure processes and mechanisms of composite coal-rock specimens," *Scientific Reports*, vol. 10, no. 1, p. 13422, 2020.

[26] H. Y. Yang, S. G. Cao, Y. Li, C. M. Sun, and P. Guo, "Soft roof failure mechanism and supporting method for gob-side entry retaining," *Minerals*, vol. 5, no. 4, pp. 707–722, 2015.

[27] S. Y. Wu, Q. W. Zhu, M. Yun, T. C. Li, Q. G. Xu, and H. Y. Guo, "Support technology of limestone roof roadway in Qiuji coal mine," *Coal mine safety*, vol. 51, pp. 93–99, 2020.

[28] Y. J. Wang, Y. B. Gao, E. Y. Wang, M. C. He, and J. Yang, "Roof deformation characteristics and preventive techniques using a novel non-pillar mining method of gob-side entry retaining by roof cutting," *Energies*, vol. 11, no. 3, p. 627, 2018.

[29] G. R. Feng and P. F. Wang, "Stress environment of entry driven along gob-side through numerical simulation incorporating the angle of break," *International Journal of Mining Science and Technology*, vol. 30, no. 2, pp. 189–196, 2020.

[30] P. Singh, A. J. S. Spearing, K. V. Jessu, and P. C. P. da Silva Ribeiro, "Establishing the need to model the actual state of stress along rock bolts," *International Journal of Mining Science and Technology*, vol. 30, no. 3, pp. 279–286, 2020.

[31] W. T. Li, N. Yang, T. C. Li, Y. H. Zhang, and G. Wang, "A new approach to simulate the supporting arch in a tunnel based on improvement of the beam element in FLAC3D," *Journal of Zhejiang University Science A: Applied Physics & Engineering*, vol. 18, no. 3, pp. 179–193, 2017.

[32] Y. G. Zhang, Z. Zhang, and S. Xue, "Stability analysis of a typical landslide mass in the Three Gorges Reservoir under varying reservoir water levels," *Environmental Earth Sciences*, vol. 79, no. 1, 2020.

[33] Z. Quan, M. He, J. Wang et al., "Instantaneous expansion with a single fracture: a new directional rock- breaking technology for roof cutting," *International Journal of Rock Mechanics & Mining Sciences*, vol. 132, p. 104399, 2020.

[34] H. Guo, L. Yuan, B. T. Shen, Q. D. Qu, and J. H. Xue, "Mining-induced strata stress changes, fractures and gas flow dynamics in multi-seam longwall mining," *Rock Mechanics and Mining Sciences*, vol. 54, pp. 129–139, 2012.

[35] D. D. Chen, F. L. He, S. R. Xie, and J. C. Zeng, "Time-space relationship between periodic fracture of plate structure of main roof and rebound in whole region with elastic foundation boundary," *Chinese Journal of Rock Mechanics and Engineering*, vol. 38, pp. 1172–1187, 2018.

[36] Y. T. Du, T. C. Li, W. T. Li, Y. D. Ren, G. Wang, and P. He, "Experimental study of mechanical and permeability behaviors during the failure of sandstone containing two preexisting fissures under triaxial compression," *Rock Mechanics and Rock Engineering*, vol. 53, no. 8, pp. 3673–3697, 2020.